NANO LETTERS

pubs.acs.org/NanoLett Letter

Cytoplasm Hydrogelation-Mediated Cardiomyocyte Sponge Alleviated Coxsackievirus B3 Infection

Jingzhe Wang,[#] Tonggong Liu,[#] Siyao Gu,[#] Hui-hui Yang, Weidong Xie,[*] Cheng Gao,[*] and Dayong Gu[*]

Cite This: https://doi.org/10.1021/acs.nanolett.3c01983 Read Online

ACCESS | Metrics & More | Article Recommendations | Supporting Information

ABSTRACT: Viral myocarditis (VMC), commonly caused by coxsackievirus B3 (CVB3) infection, lacks specific treatments and leads to serious heart conditions. Current treatments, such as IFNα and ribavirin, show limited effectiveness. Herein, rather than inhibiting virus replication, this study introduces a novel cardiomyocyte sponge, intracellular gelated cardiomyocytes (GCs), to trap and neutralize CVB3 via a receptor−ligand interaction, such as CAR and CD55. By maintaining cellular morphology, GCs serve as sponges for CVB3, inhibiting infection. *In vitro* results revealed that GCs could inhibit CVB3 infection on HeLa cells. *In vivo*, GCs exhibited a strong immune escape ability and effectively inhibited CVB3-induced viral myocarditis with a high safety profile. The most significant implication of this study is to develop a universal antivirus infection strategy via intracellular gelation of the host cell, which can be employed not only for treating defined pathogenic viruses but also for a rapid response to infection outbreaks caused by mutable and unknown viruses.

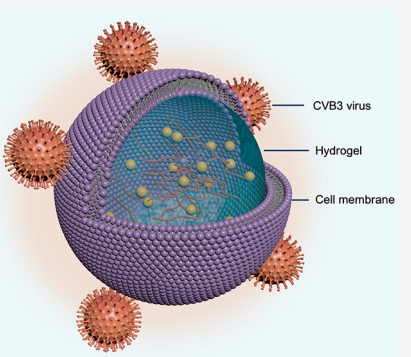

KEYWORDS: *antiretroviral strategy, coxsackievirus B3, hydrogel, virus neutralization, cellular sponge*

Group B coxsackievirus (CVB), part of a small RNA family, leads to life-threatening inflammatory diseases, especially in infants.[1] CVB comprises six different serotypes (CVB1−CVB6) and is a significant human pathogen responsible for febrile illnesses, as well as diseases affecting the heart, pancreas, and central nervous system.[2−4] Among these serotypes, CVB3 is one of the most common viruses that cause viral myocarditis (VMC), a leading cause of dilated cardiomyopathy and sudden cardiac death.[5] Current treatments for VMC rely on broad-spectrum antivirals and supportive care.[6] Broad-spectrum antiviral drugs work by targeting the virus envelope, capsid protein, and polymerase to inhibit viral replication. However, their nonspecific property and off-target effect may lead to significant side effects.[7−9] Due to the capacity of antibodies to specifically recognize and bind to viral surface antigens, the development of antiviral antibodies has become a primary focus in current scientific research.[10−12] Although antibody therapy possesses excellent specificity, it also has significant limitations. The rapid mutation of viruses may hamper the efficacy of a single antibody when confronting virus mutation or coinfection with multiple viruses.[13,14] Furthermore, the production of antibodies is typically time-consuming and costly, with the speed of production often unable to keep up with the pace of viral mutation.[15,16] Supportive care leans on the patient's immunity, which can burden those with weakened immunity.[17] Therefore, the search for an effective treatment for VMC remains a significant challenge.

CVB3 infects host cells through receptor-mediated endocytosis,[18] and coxsackievirus and adenovirus receptors (CAR) are highly expressed on the surface of susceptible target cells for CVB3 infection. CAR acts as a universal stripping receptor that binds to surface depressions (canyons) on the capsid apex of the CVB3 dodecahedron, releasing liposomes that are hidden within the hydrophobic pocket formed by the capsid protein VP1.[19,20] The liposome, known as "pocket factor", is derived from host cells and can promote the destabilization and disintegration of viral particles.[21] With the development of biomimetic nanomedicine, it has been widely reported that the host cell membrane was isolated to coat the nanomaterial and inherit the membrane function of the source cell. Due to the specific recognition between the virus and host cell, these membrane-coated nanomedicines were explored to bind and neutralize the virus for antivirus therapy.[22−25] However, the membrane separation from the host cell and reassembly process on templated nanomaterial involved protein loss and spatial disorder, which diminished the adsorption efficiency of membrane-coated nanomedicine to viruses. Additionally, the heterogeneity of nanomaterials could trigger an immune

Received: May 30, 2023
Revised: August 27, 2023

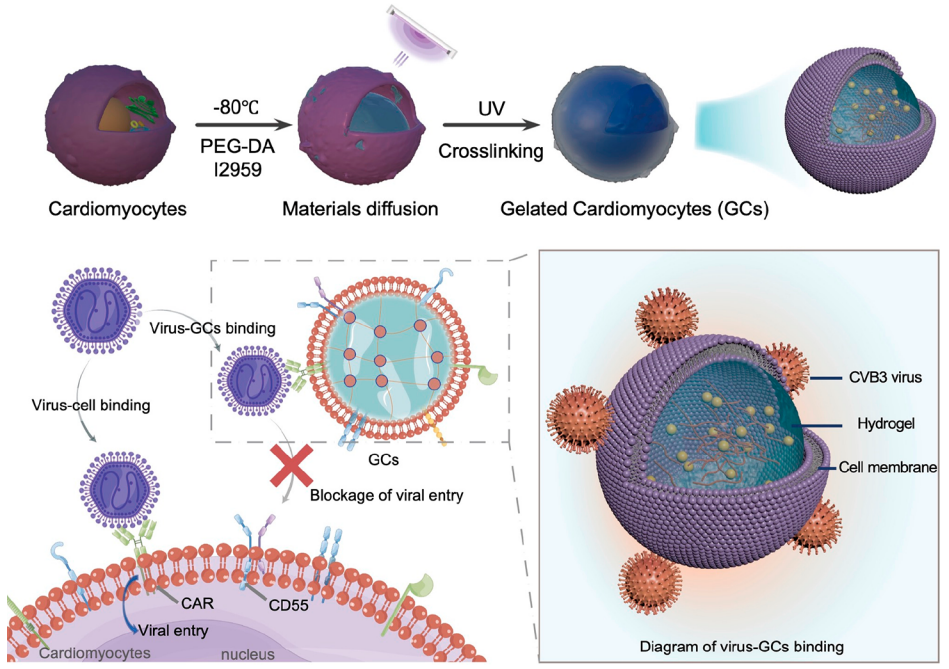

Figure 1. Schematic illustration of GCs inhibiting CVB3 infectivity. GCs were prepared through intracellular hydrogelation to preserve the intact cellular morphology and membrane structure. Benefiting from surface crucial antigens, such as CAR and CD55 receptors, GCs were disguised as cardiomyocyte-like cells and competitively bound CVB3 to immobilize the virus and prevent further infection of host cells. GCs acted as virus decoys to inhibit *in vivo* CVB3 infectivity, and the technology of intracellular gelation on the host cell provided a new insight into neutralizing the corresponding virus without screening the specific neutralizing antibody.

response and cause various side effects. Therefore, a new generation of biomimetic cells with intact membrane structure holds the potential to efficiently neutralize the virus.

To quickly respond to virus infection outbreaks, this study developed a novel cellular sponge for virus sequestration and clearance based on specific recognition of host cells by viruses, without defining any specific receptor in the host cell membrane (Figure 1). Regarding the selective infection of CVB3, the hydrogel was prepared in cardiomyocyte cytoplasm to construct GCs. Hydrogel served as an ideal cytoskeletal structure to preserve the intact morphology and membrane protein structure of host cells while eliminating the proliferation and pathogenicity ability. Subcutaneously, GCs adsorbed viruses through specific membrane receptor-mediated recognition, such as CAR and CD55,[3,26] as well as other unidentified receptors. Instead of endocytosis through receptors, viruses attached on the GC surface lost the infection ability to normal host cells, and the *in vitro* attenuation effect of GCs was evaluated in CVB3-infected cardiomyocyte. Due to the maintenance of cell morphology, GCs camouflaged themselves from the mononuclear phagocytic system and exhibited a good systemic safety profile. In a mouse model of viral myocarditis, the therapeutic efficacy of GCs was verified against CVB3-induced VMC. The development of GCs based on cellular sponges, rather than directly inhibiting virus replication, offers a rapid and effective antiviral therapy strategy, which only needed to select appropriate host cells according to the corresponding virus type. Moreover, it is particularly promising in response to large-scale infections caused by rapidly spreading viruses like COVID-19, even when the specific virus receptor is unknown.

PEG-DA and Irgacure 2959 (I2959) are commonly used for photochemical cross-linking of hydrogels.[27] This study transferred the cross-linking process into the intracellular cytoplasm. To maximize intracellular infiltration and minimize interference to cardiomyocytes, we employed PEG-DA with a low molecular weight (600 Da) and I2959 at a low concentration (10%, wt %). Successful cross-linking of PEG-DA and I2959 was achieved after UV (365−370 nm) irradiation at 6 W for 15 min, while a mixture without UV irradiation failed to form a hydrogel (Figure S1). Cardiomyocytes were chosen as host cells to construct GCs via intracellular gelation due to their highly selective recognition and susceptibility to CVB3 infection. Previous reports have indicated that frozen dead cells also serve as drug carriers for targeted delivery due to the interaction between the membrane receptor and cytokines or chemokines at the lesion site.[28] Therefore, alongside the construction of GCs, dead cells were obtained via a freezing−thaw cycle and used as nongelated dead cells (NGDs) for comparison. HL-1 in the logarithmic growth phase was treated with PEG-DA and I2959 after a freezing−thaw cycle to enhance the intracellular infiltration. Subsequently, these cells were placed on ice and exposed to ultraviolet light (UV) to construct GCs. The low-temperature condition was implemented to prevent protein degradation and the denaturation of GCs. After 24 h of storage in PBS solution at room temperature, GCs retained an intact cellular morphology (Figure 2A), similar to that of live cells. This outcome indicated that the intracellular hydrogel effectively maintained a stable cellular structure and cytoskeleton. HL-1 cells treated with PEG-DA and I2959 without UV irradiation failed to form GCs. Moreover, NGDs could not retain an intact morphology and rapidly degraded into cell fragments at room temperature. Scanning electron microscopy (SEM) results further corroborated the similarity in morphology between GCs and live cells, while transmission electron microscopy (TEM) displayed the successful intracellular gelation of GCs (Figure 2B and 2C). DiD membrane staining revealed that GCs possessed an intact

https://doi.org/10.1021/acs.nanolett.3c01983
Nano Lett. XXXX, XXX, XXX−XXX

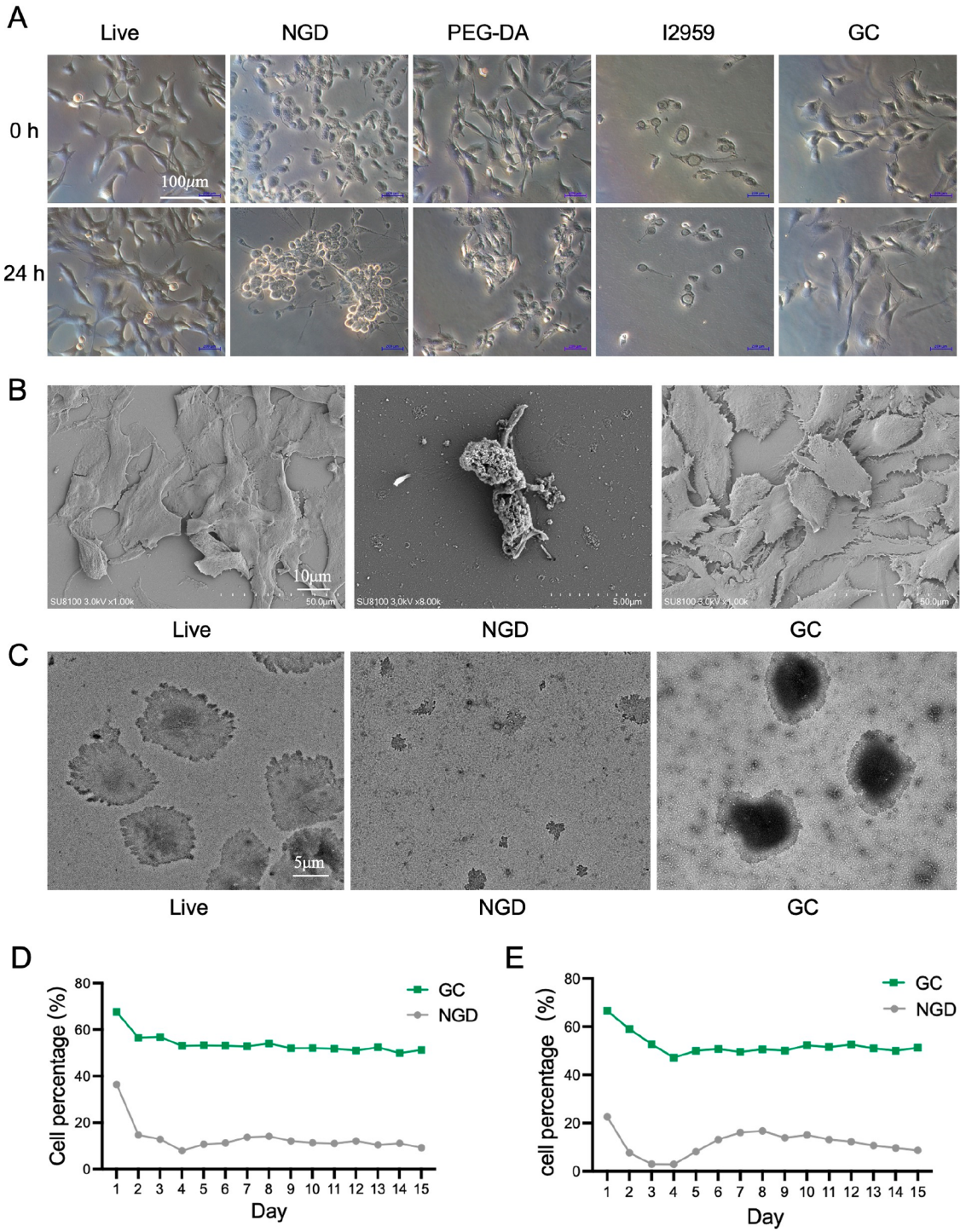

Figure 2. Engineering and characterization of GCs. (A) Representative microscopic images of the Live group, NGD group, PEG-DA group, I2959 group, and GC group. Each group of cells, except for the Live group, was incubated in PBS for 24 h. (B) Scanning electron microscopy (SEM) images of Live cells, NGDs, and GCs. (C) Transmission electron microscopy (TEM) images of Live cells, NGDs, and GCs. (D, E) Stability of GCs in 1 × PBS over a span of 15 days at room temperature (D) and through repeated freezing−thaw cycles (E), determined by flow cytometry. NS = nonsignificant, $^{**}P \leq 0.01$ and $^{***}P \leq 0.001$.

fluorescent membrane structure, whereas NGDs exhibited scattered and agglomerated cell membrane fragments and missed nuclei (Figure S2A). Cell diameter measurements indicated that the size of the GCs was consistent with that of live cells (Figure S2B). Flow cytometry results demonstrated a similar plot distribution between GCs and live cells, while NGDs appeared fragmented (Figure S2C). To ensure the stability of GCs under different conditions, GCs were stored at room temperature and subjected to repeated freezing and thawing at −80 °C for 15 days, respectively. The results indicated that GCs maintained their cellular structure regardless of storage at room temperature or under frozen conditions (Figure 2D,E). Collectively, these results suggested

https://doi.org/10.1021/acs.nanolett.3c01983
Nano Lett. XXXX, XXX, XXX−XXX

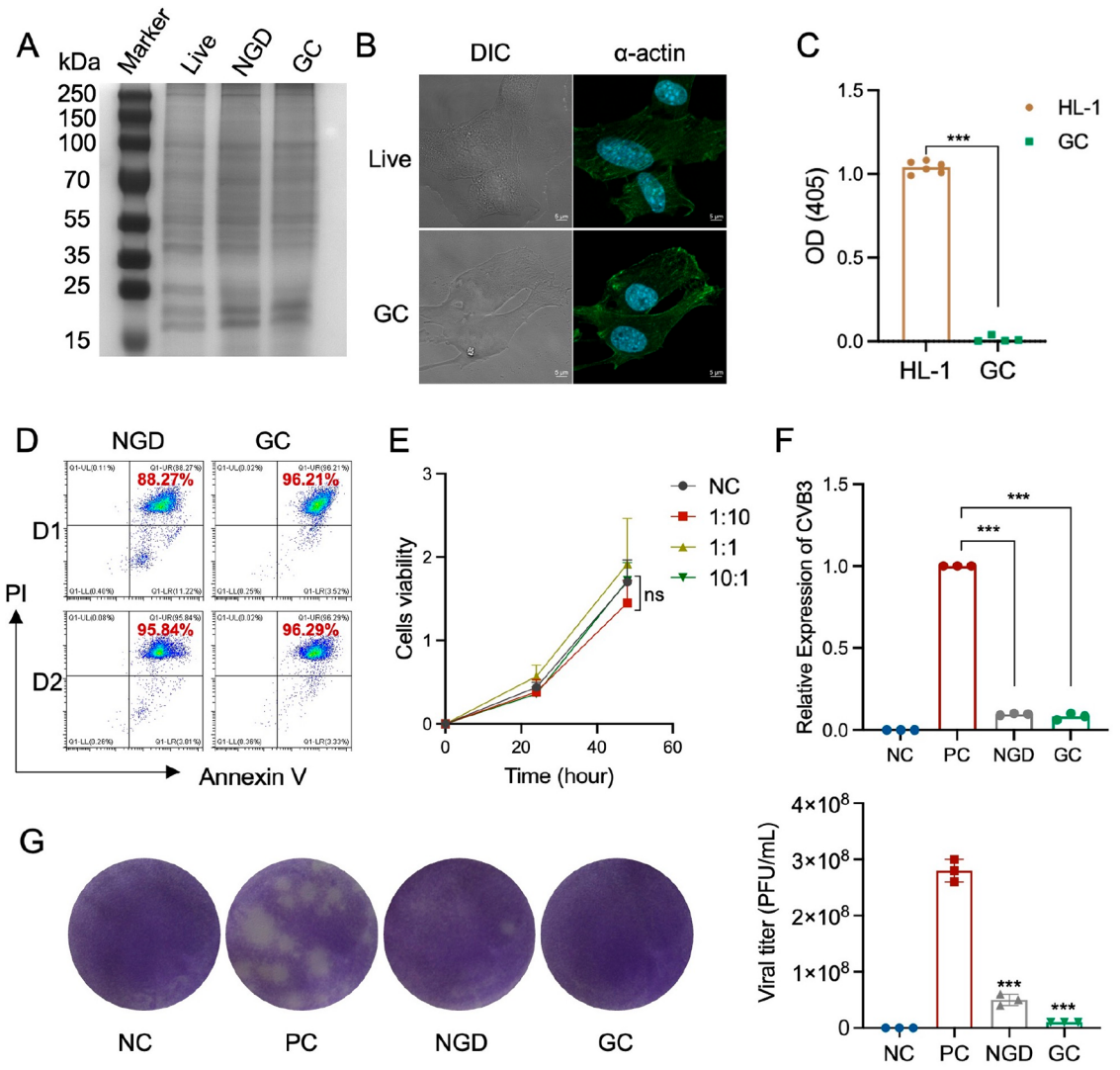

Figure 3. GCs inhibit CVB3 infection in normal host cells. (A) Coomassie blue analysis using SDS-PAGE in Live cells, NGDs, and GCs. (B) Immunofluorescent staining for α-actin. (C) Proliferation curves of HL-1 cells and GCs assessed by a CCK8 assay at 24 h. (D) Cell death detected by Annexin V/PI double staining and flow cytometry. (E) Effect of different doses of GCs (number ratio between GC and HL-1 cell, 1:10, 1:1, and 10:1) on HL-1 cell proliferation assessed by the CCK8 assay at 0, 24, and 48 h. (F) RT-PCR detection of CVB3 RNA levels in HeLa cells with or without the addition of NGDs and GCs. NC: Negative control. PC: Positive control with CVB3. (G) Plaque morphology of CVB3 on HeLa cells with or without the addition of NGDs and GCs. PFU: Plaque-forming units. NS = not significant, $^{**}P \leq 0.01$ and $^{***}P \leq 0.001$.

that GCs possess intact cell morphology, good structural stability, and storage properties *in vitro*.

To investigate protein loss in intracellular gelation, the protein profile of GCs was analyzed using SDS-PAGE. The results revealed that the protein band of GCs was almost consistent with that of live cells (Figure 3A), corroborated by BCA results (Figure S3A). Cardiomyocyte skeletal protein α-actin was examined using immunofluorescence, displaying consistency with live cells and undamaged protein structural domains (Figure 3B). The CCK8 assay results showed that GCs had no proliferative ability (Figure 3C). Annexin−V-PI staining revealed that GCs were dead cells, while all cells in the NGD group died, with a normal cell mortality rate of about 8.75% after 1 day (Figures 3D and S3B). HL-1 cell viability with different GC proportions (1:10, 1:1, and 10:1) revealed good biocompatibility (Figure 3E). HeLa and HL-1 cells were incubated with 100 TCID50 CVB3 and 1×10^6 GCs for 2 h to check whether GCs could neutralize CVB3 and protect those host cells. After 24 h, GCs in the supernatant were removed, and the mRNA level of CVB3 in cells was detected by a real-time fluorescence quantitative polymerase chain reaction (RT-PCR). The results indicated that HeLa and HL-1 cells were easily infected with CVB3, while GCs significantly reduced the expression of CVB3 mRNA in both cell types, indicating that GCs inhibited CVB3 infection (Figures 3F and S3C). Additionally, the cell fragments in the NGD group also exhibited a similar inhibition effect against CVB3 infection. Viral plaque results showed reduced viral plaques in both NGD and GC groups compared to the PC group, due to GCs binding and neutralizing CVB3, inhibiting its infection (Figure 3G). Additional antiviral experiments with GCs diluted at 1/2 concentration showed that 1×10^6 GCs coincubated with HeLa cells completely inhibited CVB3 infection, in a concentration-dependent manner (Figure S3D). To rule out the possibility of physical barrier effects by GCs, we preincubated GCs with the virus for 30 min, collected the supernatant, and infected HeLa cells. GCs still effectively inhibited the CVB3 virus infection (Figure S3E). Overall, the

https://doi.org/10.1021/acs.nanolett.3c01983
Nano Lett. XXXX, XXX, XXX−XXX

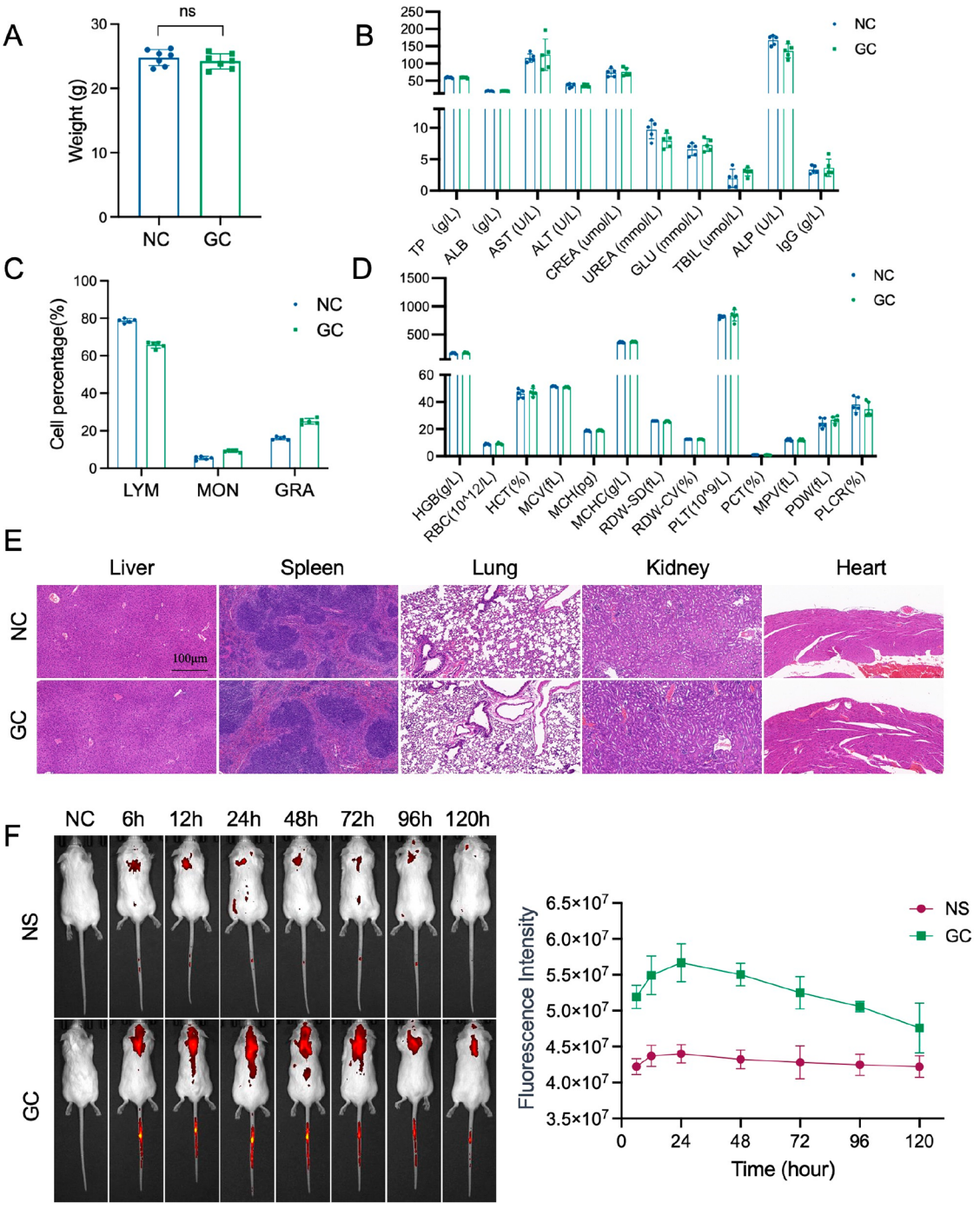

Figure 4. *In vivo* safety assessment of GCs. (A) Balb/c mice were intravenously injected with 1×10^6 GCs every 2 days with a total of four doses (n = 5), and the body weight was recorded at experimental end points (day 7). (B) Comprehensive serum chemistry analysis was performed at day 7. Measurement parameters included TB (total bilirubin), ALB (albumin), AST (aspartate aminotransferase), ALT (alanine aminotransferase), CREA (creatinine), UREA (blood urea nitrogen), GLU (glucose), TBIL (total bilirubin), ALP (alkaline phosphatase), and IgG (immunoglobulin G). (C) Lymphocyte (LYM), monocyte (MON), and granulocyte (GRA) counts were detected at day 7. (D) Complete blood count collected from GC group mice was analyzed at day 7. The detected items included HGB (hemoglobin), RBC (red blood cells), HCT (hematocrit), MCV (mean corpuscular volume), MCH (mean corpuscular hemoglobin), MCHC (mean corpuscular hemoglobin concentration), RDW (red cell distribution width), PLT (platelets), PCT (platelet crit), MPV (mean platelet volume), PDW (platelet distribution width), and PLCR (platelet crit-to-large cell ratio). (E) Histopathological analysis of the heart, liver, spleen, lung, and kidney using H&E-stained tissue sections. Scale bar: 100 μm. (F) Mice were intravenously (i.v.) injected with NS and GCs at a number of 1×10^6 cells per mouse, and the fluorescence signals were detected using an *in vivo* imaging system (D-22 cm) after administration at 6, 12, 24, 48, 72, 96, and 120 h (n = 7). NS = nonsignificant, $^{**}P \leq 0.01$ and $^{***}P \leq 0.001$.

results suggest that GCs maintain the host cell cytoskeleton and efficiently preserve membrane proteins, neutralizing the CVB3 virus and suppressing infection. The replication and infection processes of CVB3 are complex, including interaction between virus particles and host receptors, fusion of a virion envelope and cell membrane, nucleocapsid decapitation, and release of the RNA genome into the cytoplasm. Obviously, the *in vitro* anti-infection effect of GCs was mainly through binding

https://doi.org/10.1021/acs.nanolett.3c01983
Nano Lett. XXXX, XXX, XXX−XXX

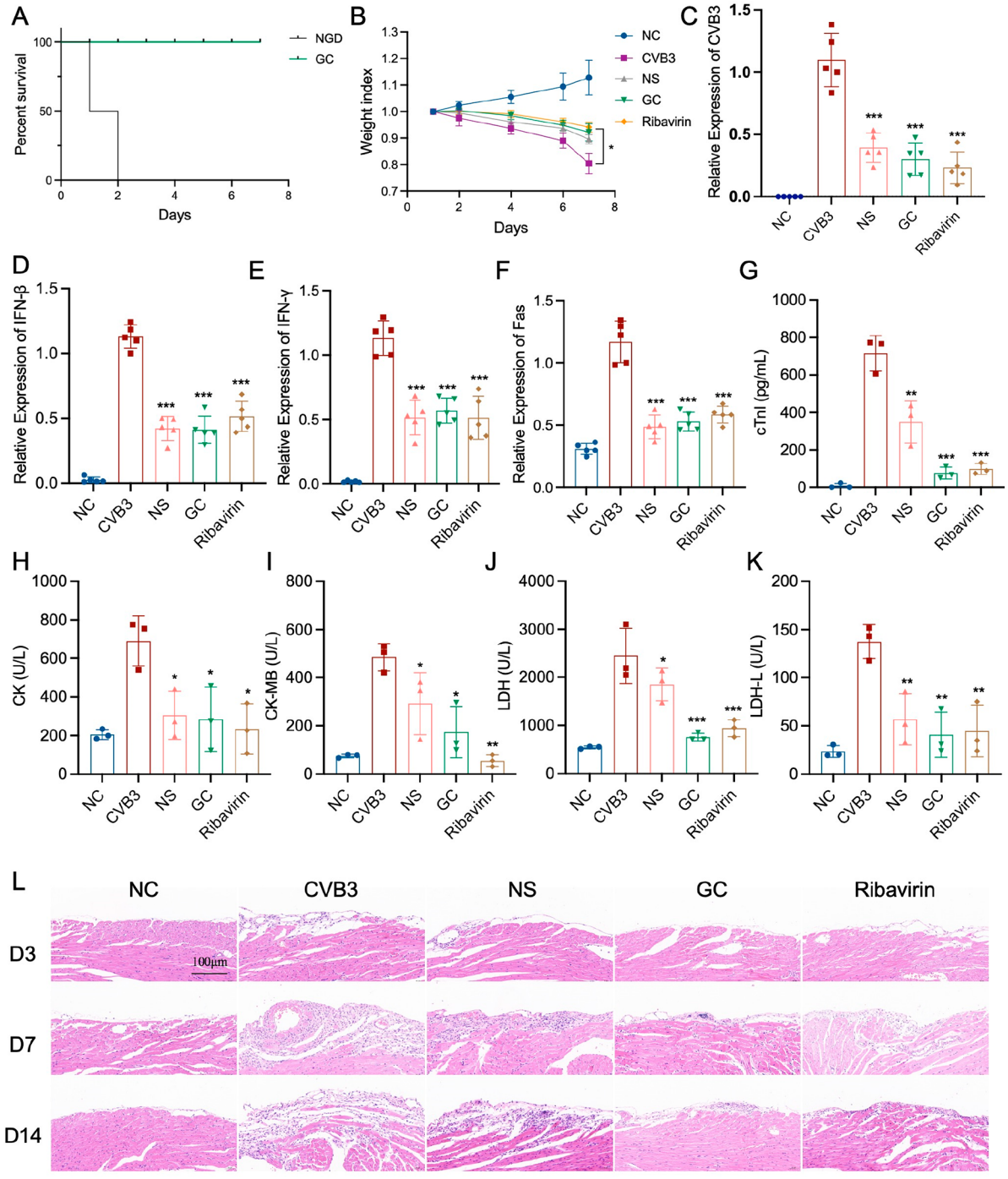

Figure 5. *In vivo* therapy of GCs against CVB3 infection. (A) Survival rates of CVB3-infected mice after iv injection with NGDs and GCs (n = 5). (B) CVB3-infected mice were iv administered with 100 μL of PBS (100 μL per mouse), NS (prepared from 1×10^7 cardiomyocytes), GCs (1×10^6), and Ribavirin (50 mg/kg), every other day for a total of 7 injections, and body weight change curves of mice were created (n = 7). (C) RT-PCR detection of CVB3 RNA levels in the heart. (D−F) RT-PCR detection of IFN-β, IFN-γ, and Fas mRNA levels in the heart. (G) ELISA detects serum cTnI levels. (H−K) Serum CK, CK-MB, LDH, and LDH-L analyses were performed on day 7. (L) Histopathological analysis of the heart, liver, spleen, lung, and kidney using H&E-stained tissue sections on day 3, day 7, and day 14. *$P \leq 0.05$, **$P \leq 0.01$, and ***$P \leq 0.001$.

and neutralizing the virus and then immobilizing it to inhibit further interaction between virus particles and receptors of the host cell. Of note, the virus could be not replicated after being attached on the GC surface due to the noncell viability.

The potential systemic biosafety of GCs is a significant concern for clinical translation, as an intracellular hydrogel may induce physiological toxicity and immunogenicity. To evaluate acute toxicity, Balb/c mice received intravenous injections of 1 $\times 10^6$ GCs every other day for 5 doses, with no apparent side effects or weight differences observed in both normal and GC-treated mice (Figure 4A). Comprehensive blood tests and serum analyses confirmed consistent levels of virus-infection-related biomarkers (ALT and AST) between GC-treated and control groups (Figure 4B). Lymphocyte (LYM) proportions decreased, while monocyte (MON) and granulocyte (GRA) proportions increased during CVB3 infection.[29] Our examina-

https://doi.org/10.1021/acs.nanolett.3c01983
Nano Lett. XXXX, XXX, XXX−XXX

tion of lymphocytes, monocytes, and granulocytes (Figure 4C) and other blood biomarkers (Figure 4D) showed no significant differences between GCs and control groups. These results confirm the short-term safety of GCs. Histopathological analysis of collected organs (heart, liver, spleen, lung, and kidney) showed no immune infiltration, lesion formation, or tissue injury in GC-treated mice (Figure 4E), indicating good *in vivo* biocompatibility. To track the *in vivo* biological distribution, we stained HL-1 cells with DiD before intracellular gelation and prepared them into nanoparticle cells (NS) and GCs. Live imaging revealed that the GC group exhibited the strongest fluorescence signal at 24 h, gradually decreasing after 48 h. In contrast, the fluorescence intensity of the NS group, prepared with the same cell quantity, was significantly lower than that of the GC group (Figure 4F). GCs first entered the lungs at 6 h and then moved to the liver and spleen for metabolism. By 72 h, GCs' fluorescence intensity noticeably reduced. Conversely, the NS group's fluorescence intensity rapidly declined after 24 h (Figure S4A). These results suggest that GCs have a long circulation time, sufficient to achieve adequate virus neutralization, and may transport captured viruses to organs, such as the lungs, liver, and spleen for metabolism and elimination. Although our small-scale preliminary safety study met the requirements for acute *in vivo* toxicity in VMC mice over 7 days, further exploration is still needed to investigate the long-term toxicity of GCs on a larger scale.

As a novel cellular decoy, we investigated the antiviral efficacy of GCs in CVB3-infected mice. CVB3-induced viral myocarditis peaks at day 7 and gradually decreases.[30] To construct the viral myocarditis model, we intraperitoneally injected mice with 1×10^5 TCID50 CVB3. We first conducted a comparative analysis of the *in vivo* biosafety of NGDs and GCs. The results indicated that all mice in the NGD group succumbed 1 day postadministration (Figure 5A), possibly due to the cell fragments inducing a pulmonary embolism.[31,32] In contrast, the GC group showed no fatalities, indicating higher biosafety. Therefore, despite that NGDs exhibit effective viral neutralization capabilities *in vitro*, their biosafety is considerably low. Subsequently, we tested the *in vivo* antiviral capabilities of GCs. Mice were divided into five groups: the NC, CVB3, NS, GCs, and Ribavirin groups. Each group of mice received an injection every other day, for a total of 7 injections. On day 2 after CVB3 inoculation, mice in the CVB3 group experienced rapid body weight decline, whereas the NS, GC, and Ribavirin groups exhibited improved body weight trends (Figure 5B). On day 7, we evaluated the CVB3 viral load and IFN-β, IFN-γ, and Fas expression levels related to myocardial cell damage and serum indicators closely related to viral infection (cTnI, CK, CK-MB, LDH, and LDH-L). The CVB3 group showed significantly increased myocardial injury-related indicators. In contrast, the NS, GC, and Ribavirin groups exhibited reduced viral titers and alleviated myocardial cell damage. Specifically, the antiviral effect of the GC group was close to that of the Ribavirin group. Additionally, the GC group showed significantly reduced AST and ALT levels and an increased proportion of monocytes and neutrophils in the peripheral blood (Figure S5A and S5B), effectively alleviating viral myocarditis. No significant changes were observed in other blood parameters (Figures S5C and S5D). Notably, although NS inhibited CVB3-induced viral myocarditis, the dosage difference between GCs and NS means that GCs could significantly enhance the neutralizing efficiency against the virus. Finally, we collected the heart, liver, spleen, lungs, and kidneys of mice on days 3, 7, and 14 for pathological analysis. The GC group effectively improved CVB3-induced viral myocarditis, with an inhibitory effect comparable to the Ribavirin group (Figure 5L). H&E staining of the liver, spleen, lungs, and kidneys in all groups was similar to that of normal mice, with no evidence of pathological changes or tissue damage (Figure S6).

Biological neutralization represents an emerging antiviral infection strategy developed in recent years. Up to now, the technology of utilizing cell-membrane-coated nanoparticles has been applied to the neutralization of various viruses,[33] such as HIV,[25] the Zika virus,[24] and SARS-CoV-2.[34] In addition, biological neutralization including a neutralizing antibody demonstrated therapeutic effectiveness, through binding to a cell-free virus and preventing it from infecting cells.[35,36] However, the main challenge relies on the slow development rate of neutralizing antibodies, and the time-consuming process leads to an inadequately rapid response to virus spread. The envelope or capsid proteins of the virus primarily recognized the specific receptors on the host cell membrane, facilitating virus attachment, endocytosis, and replication.[37] Based on the virus infection characterization of the receptor−ligand interaction,[38] a host membrane camouflaged strategy was developed as a decoy to competitively absorb the virus and prevent further virus infection. For example, the $CD4^+$ T cell membrane was collected to encapsulate PLGA nanoparticles, and membranes CXCR4 and CCR5 specifically bound HIV gp120 to neutralize HIV and inhibit $CD4^+$ T cell apoptosis.[25] The Zika virus is a mosquito-borne virus causing neurological disorders and congenital disabilities such as microcephaly, and the biomimetic mosquito C6/36 cell membrane coated gelatin nanoparticles neutralized the Zika virus, reducing fetal microcephaly by preventing the virus from crossing the placental blood barrier.[24] CD147 has been identified as a receptor for SARS-CoV-2. Biomimetic nanoparticles derived from the membrane of SARS-CoV-2-susceptible human pulmonary epithelial type II cells or human macrophages show a dose-dependent inhibitory effect on the infectivity of SARS-CoV-2.[34] In summary, cell membrane biomimetic nanomedicine has been proven to be a unique and effective approach for neutralizing viruses.

However, the construction process of membrane-coated nanomedicine involves cell disruption and membrane separation and subsequent membrane coating and reassembly on template nanoparticles, which can induce membrane protein loss and spatial disorder. As a result, the domain responsible for virus binding may be hindered or disrupted, reducing the adsorption capacity of the biomimetic nanomedicines. In addition, incomplete membrane-coated nanomedicine enhanced the risk of systemic clearance by monocyte phagocytosis as "foreign substances". Therefore, it is crucial to ensure that the cell membrane structure and physiological characteristics are not damaged during the preparation of a biomimetic nanomedicine. To overcome these limitations, we prepared a biocompatible hydrogel as an ideal cytoskeleton to stabilize the morphology and membrane protein of virus-susceptible cells and enhance their absorption efficiency for antiviral neutralization. *In vivo* safety evaluation and biodistribution demonstrated that GCs had excellent biocompatibility, immune evasion capability, and prolonged retention time in the infected tissue. HL-1 cells derived from mouse hearts possessed a strong affinity to bind CVB3, and

https://doi.org/10.1021/acs.nanolett.3c01983
Nano Lett. XXXX, XXX, XXX−XXX

intracellular gelation technology was employed to construct a cell sponge to capture and neutralize systemic and localized CVB3 and prevent further infection on cardiomyocytes. In our future research, we aim to engineer antibody receptors by gene manipulation. Specifically, we plan to express the Fab fragments of highly effective virus-neutralizing antibodies on the surface of GCs through genetic engineering, thereby enabling the adsorption and disintegration of viruses. This will further improve the adsorption capacity of GCs and facilitate virus capture and neutralization.

This study emphasizes the use of cardiomyocytes in preclinical exploratory research. It is noteworthy that during the clinical translation phase autologous or allogeneic cardiac myocytes may face complex challenges such as difficulties in harvesting and immune rejection. As a result, alternative cells may become a highly prospective solution. Our research's core concept focuses on utilizing the high specificity of host cells to adsorb and neutralize viruses, providing potential alternatives for other cells with similar high-affinity characteristics. Overall, the primary contribution of this study is the introduction of an innovative antiviral strategy based on intracellular gelation. This strategy, rooted in the unique features of intracellular gel technology, can effectively overcome the "high-pressure selection" mutation challenges that traditional antiviral methods find difficult to address. Even if the virus mutates, its recognition pattern may remain relatively stable, thereby reducing the risk of the virus escaping neutralization. Facing the outbreak of an epidemic, especially when viruses spread and mutate rapidly, the development cycle of traditional drugs and vaccines may be prolonged, making them less suitable for a rapid response. However, the intracellular gelation strategy proposed in this study, due to its rapid applicability, can be deployed and promoted in a short time, making it a swift antiviral response solution. By employing intracellular gelation in host cells, we have not only demonstrated an innovative and promising antiviral technology but also, more importantly, provided a universal and practically feasible solution for handling urgent epidemic outbreaks, such as those similar to COVID-19.

■ ASSOCIATED CONTENT

Supporting Information

The Supporting Information is available free of charge at https://pubs.acs.org/doi/10.1021/acs.nanolett.3c01983.

Experimental materials and methods as well as supplementary figures, including characterization of hydrogels, SEM images of GCs, cell death in a live cell group, CVB3 RNA levels in HL-1 cells with or without the addition of NGDs and GCs, plaque morphology of CVB3 in HeLa cells with or without GCs, *in vivo* metabolism and distribution of GCs, serological analysis, and results of H&E pathological analysis (PDF)

■ AUTHOR INFORMATION

Corresponding Authors

Weidong Xie − *Shenzhen Key Laboratory of Health Science and Technology, Institute of Biopharmaceutical and Health Engineering, Shenzhen International Graduate School, Tsinghua University, Shenzhen 518055, China*; Email: xiewd@sz.tsinghua.edu.cn

Cheng Gao − *Department of Laboratory Medicine, Shenzhen Institute of Translational Medicine, The First Affiliated Hospital of Shenzhen University, Shenzhen Second People's Hospital, Shenzhen Key Laboratory of Medical Laboratory and Molecular Diagnostics, Shenzhen 518035, China*; Email: chenggao@email.szu.edu.cn

Dayong Gu − *Department of Laboratory Medicine, Shenzhen Institute of Translational Medicine, The First Affiliated Hospital of Shenzhen University, Shenzhen Second People's Hospital, Shenzhen Key Laboratory of Medical Laboratory and Molecular Diagnostics, Shenzhen 518035, China*; orcid.org/0000-0002-9547-8474; Email: wanhood@email.szu.edu.cn

Authors

Jingzhe Wang − *Department of Laboratory Medicine, Shenzhen Institute of Translational Medicine, The First Affiliated Hospital of Shenzhen University, Shenzhen Second People's Hospital, Shenzhen Key Laboratory of Medical Laboratory and Molecular Diagnostics, Shenzhen 518035, China; Shenzhen Institute of Synthetic Biology, Shenzhen Institute of Advanced Technology, Chinese Academy of Sciences, Shenzhen 518055, China*

Tonggong Liu − *Department of Laboratory Medicine, Shenzhen Institute of Translational Medicine, The First Affiliated Hospital of Shenzhen University, Shenzhen Second People's Hospital, Shenzhen Key Laboratory of Medical Laboratory and Molecular Diagnostics, Shenzhen 518035, China*

Siyao Gu − *Shenzhen Key Laboratory of Health Science and Technology, Institute of Biopharmaceutical and Health Engineering, Shenzhen International Graduate School, Tsinghua University, Shenzhen 518055, China*

Hui-hui Yang − *Department of Laboratory Medicine, Shenzhen Institute of Translational Medicine, The First Affiliated Hospital of Shenzhen University, Shenzhen Second People's Hospital, Shenzhen Key Laboratory of Medical Laboratory and Molecular Diagnostics, Shenzhen 518035, China*

Complete contact information is available at: https://pubs.acs.org/10.1021/acs.nanolett.3c01983

Author Contributions

J.W., T.L., and S.G. contributed equally to this work. Methodology: D.G., C.G., W.X. and J.W.; Experiment: J.W., T.L. and S.G.; Writing-original draft: J.W.; Writing-review and editing: T.L. and S.G.; Data curation: J.W., T.L., S.G. and H.Y.; Supervision: D.G., C.G. and W.X.; Funding acquisition: D.G., C.G. and J.W.

Author Contributions

#J.W., T.L., and S.G. contributed equally to this work. Methodology: D.G., C.G., W.X., and J.W. Experiment: J.W., T.L., and S.G. Writing-original draft: J.W. Writing-review and editing: T.L. and S.G. Data curation: J.W., T.L., S.G., and H.Y. Supervision: D.G., C.G., and W.X. Funding acquisition: D.G., C.G., and J.W.

Notes

The authors declare no competing financial interest.

■ ACKNOWLEDGMENTS

This work was supported by National Key Research and Development Program of China (2022YFC2302700), National Natural Science Foundation of China (32001016, 32371381), Guangdong Basic and Applied Basic Research Foundation

(2020A1515110871, 2022A1515220006), Guangdong Science and Technology Foundation (2021A1515220084, 2022B1111020001), China Postdoctoral Science Foundation (2022M722204), and Shenzhen Science and Technology Foundation (GJHZ20200731095604013, JSGG20220301090003004, 201906133000069, SGLH20180625171602058, JCYJ20200109120205924, RCBS20200714114856016, JCYJ20210324103204011).

REFERENCES

(1) Stone, V. M.; Hankaniemi, M. M.; Laitinen, O. H.; Sioofy-Khojine, A. B.; Lin, A.; Diaz Lozano, I. M.; Mazur, M. A.; Marjomaki, V.; Lore, K.; Hyoty, H.; et al. A hexavalent Coxsackievirus B vaccine is highly immunogenic and has a strong protective capacity in mice and nonhuman primates. *Sci. Adv.* **2020**, *6* (19), No. eaaz2433.

(2) Shih, W. L.; Tung, Y. C.; Chang, L. Y.; Fang, C. T.; Tsai, W. Y. Increased Incidence of Pediatric Type 1 Diabetes With Novel Association With Coxsackievirus A Species in Young Children but Declined Incidence in Adolescents in Taiwan. *Diabetes Care* **2021**, *44* (7), 1579−1585.

(3) Kallewaard, N. L.; Zhang, L.; Chen, J. W.; Guttenberg, M.; Sanchez, M. D.; Bergelson, J. M. Tissue-specific deletion of the coxsackievirus and adenovirus receptor protects mice from virus-induced pancreatitis and myocarditis. *Cell Host Microbe* **2009**, *6* (1), 91−98.

(4) Mohamud, Y.; Tang, H.; Xue, Y. C.; Liu, H.; Ng, C. S.; Bahreyni, A.; Luo, H. Coxsackievirus B3 targets TFEB to disrupt lysosomal function. *Autophagy* **2021**, *17* (12), 3924−3938.

(5) Weithauser, A.; Bobbert, P.; Antoniak, S.; Bohm, A.; Rauch, B. H.; Klingel, K.; Savvatis, K.; Kroemer, H. K.; Tschope, C.; Stroux, A.; et al. Protease-activated receptor-2 regulates the innate immune response to viral infection in a coxsackievirus B3-induced myocarditis. *J. Am. Coll Cardiol* **2013**, *62* (19), 1737−1745.

(6) Rivadeneyra, L.; Charo, N.; Kviatcovsky, D.; de la Barrera, S.; Gomez, R. M.; Schattner, M. Role of neutrophils in CVB3 infection and viral myocarditis. *J. Mol. Cell Cardiol* **2018**, *125*, 149−161.

(7) Liu, X.; Wang, X.; Kapteijn, F. Water and Metal-Organic Frameworks: From Interaction toward Utilization. *Chem. Rev.* **2020**, *120* (16), 8303−8377.

(8) Sainz, B., Jr.; Barretto, N.; Martin, D. N.; Hiraga, N.; Imamura, M.; Hussain, S.; Marsh, K. A.; Yu, X.; Chayama, K.; Alrefai, W. A.; et al. Identification of the Niemann-Pick C1-like 1 cholesterol absorption receptor as a new hepatitis C virus entry factor. *Nat. Med.* **2012**, *18* (2), 281−285.

(9) Voros, J.; Urbanek, A.; Rautureau, G. J.; O'Connor, M.; Fisher, H. C.; Ashcroft, A. E.; Ferguson, N. Large-scale production and structural and biophysical characterizations of the human hepatitis B virus polymerase. *J. Virol* **2014**, *88* (5), 2584−2599.

(10) Schmidt, F.; Weisblum, Y.; Muecksch, F.; Hoffmann, H. H.; Michailidis, E.; Lorenzi, J. C. C.; Mendoza, P.; Rutkowska, M.; Bednarski, E.; Gaebler, C.; et al. Measuring SARS-CoV-2 neutralizing antibody activity using pseudotyped and chimeric viruses. *J. Exp Med.* **2020**, *217* (11), No. e20201181.

(11) Chi, X.; Liu, X.; Wang, C.; Zhang, X.; Li, X.; Hou, J.; Ren, L.; Jin, Q.; Wang, J.; Yang, W. Humanized single domain antibodies neutralize SARS-CoV-2 by targeting the spike receptor binding domain. *Nat. Commun.* **2020**, *11* (1), 4528.

(12) Li, C.; Yu, D.; Wu, X.; Liang, H.; Zhou, Z.; Xie, Y.; Li, T.; Wu, J.; Lu, F.; Feng, L.; et al. Twelve-month specific IgG response to SARS-CoV-2 receptor-binding domain among COVID-19 convalescent plasma donors in Wuhan. *Nat. Commun.* **2021**, *12* (1), 4144.

(13) Bauer, G.; Struck, F.; Staschik, E.; Maile, J.; Wochinz-Richter, K.; Motz, M.; Soutschek, E. Differential avidity determination of IgG directed towards the receptor-binding domain (RBD) of SARS-CoV-2 wild-type and its variants in one assay: Rational tool for the assessment of protective immunity. *J. Med. Virol* **2022**, *94* (11), 5294−5303.

(14) Hanke, L.; Das, H.; Sheward, D. J.; Perez Vidakovics, L.; Urgard, E.; Moliner-Morro, A.; Kim, C.; Karl, V.; Pankow, A.; Smith, N. L.; et al. A bispecific monomeric nanobody induces spike trimer dimers and neutralizes SARS-CoV-2 in vivo. *Nat. Commun.* **2022**, *13* (1), 155.

(15) Guo, X.; Wen, F.; Zheng, N.; Saive, M.; Fauconnier, M. L.; Wang, J. Aptamer-Based Biosensor for Detection of Mycotoxins. *Front Chem.* **2020**, *8*, 195.

(16) Mahajan, S. P.; Ruffolo, J. A.; Frick, R.; Gray, J. J. Hallucinating structure-conditioned antibody libraries for target-specific binders. *Front Immunol* **2022**, *13*, 999034.

(17) Stergioti, E. M.; Manolakou, T.; Boumpas, D. T.; Banos, A. Antiviral Innate Immune Responses in Autoimmunity: Receptors, Pathways, and Therapeutic Targeting. *Biomedicines* **2022**, *10* (11), 2820.

(18) Chang, H.; Li, X.; Cai, Q.; Li, C.; Tian, L.; Chen, J.; Xing, X.; Gan, Y.; Ouyang, W.; Yang, Z. The PI3K/Akt/mTOR pathway is involved in CVB3-induced autophagy of HeLa cells. *Int. J. Mol. Med.* **2017**, *40* (1), 182−192.

(19) Xu, L.; Zheng, Q.; Zhu, R.; Yin, Z.; Yu, H.; Lin, Y.; Wu, Y.; He, M.; Huang, Y.; Jiang, Y.; et al. Cryo-EM structures reveal the molecular basis of receptor-initiated coxsackievirus uncoating. *Cell Host Microbe* **2021**, *29* (3), 448−462.

(20) Kicmal, T. M.; Tate, P. M.; Dial, C. N.; Esin, J. J.; Mounce, B. C. Polyamine Depletion Abrogates Enterovirus Cellular Attachment. *J. Virol* **2019**, *93* (20), No. 01054-01019.

(21) Plevka, P.; Perera, R.; Cardosa, J.; Kuhn, R. J.; Rossmann, M. G. Crystal structure of human enterovirus 71. *Science* **2012**, *336* (6086), 1274.

(22) Gao, C.; Huang, Q.; Liu, C.; Kwong, C. H. T.; Yue, L.; Wan, J. B.; Lee, S. M. Y.; Wang, R. Treatment of atherosclerosis by macrophage-biomimetic nanoparticles via targeted pharmacotherapy and sequestration of proinflammatory cytokines. *Nat. Commun.* **2020**, *11* (1), 2622.

(23) Chen, Y.; Chen, M.; Zhang, Y.; Lee, J. H.; Escajadillo, T.; Gong, H.; Fang, R. H.; Gao, W.; Nizet, V.; Zhang, L. Broad-Spectrum Neutralization of Pore-Forming Toxins with Human Erythrocyte Membrane-Coated Nanosponges. *Adv. Healthc Mater.* **2018**, *7* (13), No. 1701366.

(24) Rao, L.; Wang, W.; Meng, Q. F.; Tian, M.; Cai, B.; Wang, Y.; Li, A.; Zan, M.; Xiao, F.; Bu, L. L.; et al. A Biomimetic Nanodecoy Traps Zika Virus To Prevent Viral Infection and Fetal Microcephaly Development. *Nano Lett.* **2019**, *19* (4), 2215−2222.

(25) Wei, X.; Zhang, G.; Ran, D.; Krishnan, N.; Fang, R. H.; Gao, W.; Spector, S. A.; Zhang, L. T-Cell-Mimicking Nanoparticles Can Neutralize HIV Infectivity. *Adv. Mater.* **2018**, *30* (45), No. 1802233.

(26) Heymans, S.; Eriksson, U.; Lehtonen, J.; Cooper, L. T., Jr. The Quest for New Approaches in Myocarditis and Inflammatory Cardiomyopathy. *J. Am. Coll Cardiol* **2016**, *68* (21), 2348−2364.

(27) Rennerfeldt, D. A.; Renth, A. N.; Talata, Z.; Gehrke, S. H.; Detamore, M. S. Tuning mechanical performance of poly(ethylene glycol) and agarose interpenetrating network hydrogels for cartilage tissue engineering. *Biomaterials* **2013**, *34* (33), 8241−8257.

(28) Ci, T.; Li, H.; Chen, G.; Wang, Z.; Wang, J.; Abdou, P.; Tu, Y.; Dotti, G.; Gu, Z. Cryo-shocked cancer cells for targeted drug delivery and vaccination. *Sci. Adv.* **2020**, *6* (50), No. eabc3013.

(29) Hu, Y.; Ren, J.; Dong, X.; Zhang, D.; Qu, Y.; Yang, C.; Sun, Y.; Li, J.; Luo, F.; Wang, W.; et al. Fulminant Giant Cell Myocarditis vs. Lymphocytic Myocarditis: A Comparison of Their Clinical Characteristics, Treatments, and Outcomes. *Front Cardiovasc Med.* **2021**, *8*, 770549.

(30) Tian, Y.; Gong, X.; Qin, D.; Cao, Y.; Zhang, S.; Xia, L.; Liu, F.; Su, Z. S1PR1-dependent migration of ILC3s from intestinal tissue to the heart in a mouse model of viral myocarditis. *J. Leukoc Biol.* **2023**, *114* (2), 154−163.

(31) Lee, H. S.; Kang, N. W.; Kim, H.; Kim, D. H.; Chae, J. W.; Lee, W.; Song, G. Y.; Cho, C. W.; Kim, D. D.; Lee, J. Y. Chondroitin sulfate-hybridized zein nanoparticles for tumor-targeted delivery of docetaxel. *Carbohydr. Polym.* **2021**, *253*, 117187.

https://doi.org/10.1021/acs.nanolett.3c01983
Nano Lett. XXXX, XXX, XXX−XXX

(32) Xu, Y.; Yang, Y.; Zheng, H.; Huang, C.; Zhu, X.; Zhu, Y.; Guan, R.; Xin, Z.; Liu, Z.; Tian, Y. Intracavernous injection of size-specific stem cell spheroids for neurogenic erectile dysfunction: Efficacy and risk versus single cells. *EBioMedicine* **2020**, *52*, 102656.
(33) Xiao, M.; Tian, F.; Liu, X.; Zhou, Q.; Pan, J.; Luo, Z.; Yang, M.; Yi, C. Virus Detection: From State-of-the-Art Laboratories to Smartphone-Based Point-of-Care Testing. *Adv. Sci. (Weinh)* **2022**, *9* (17), No. e2105904.
(34) Zhang, Q.; Honko, A.; Zhou, J.; Gong, H.; Downs, S. N.; Vasquez, J. H.; Fang, R. H.; Gao, W.; Griffiths, A.; Zhang, L. Cellular Nanosponges Inhibit SARS-CoV-2 Infectivity. *Nano Lett.* **2020**, *20* (7), 5570−5574.
(35) Wang, S.; Wang, D.; Duan, Y.; Zhou, Z.; Gao, W.; Zhang, L. Cellular Nanosponges for Biological Neutralization. *Adv. Mater.* **2022**, *34* (13), No. e2107719.
(36) Lanza, R.; Russell, D. W.; Nagy, A. Engineering universal cells that evade immune detection. *Nat. Rev. Immunol* **2019**, *19* (12), 723−733.
(37) Fredericksen, B. L.; Wei, B. L.; Yao, J.; Luo, T.; Garcia, J. V. Inhibition of endosomal/lysosomal degradation increases the infectivity of human immunodeficiency virus. *J. Virol* **2002**, *76* (22), 11440−11446.
(38) Gao, W.; Zhang, Y.; Zhang, Q.; Zhang, L. Nanoparticle-Hydrogel: A Hybrid Biomaterial System for Localized Drug Delivery. *Ann. Biomed Eng.* **2016**, *44* (6), 2049−2061.

https://doi.org/10.1021/acs.nanolett.3c01983
Nano Lett. XXXX, XXX, XXX−XXX

Supporting Information

Cytoplasm hydrogelation-mediated cardiomyocyte sponge alleviated coxsackievirus B3 infection

Jingzhe Wang[1,2,#], Tonggong Liu[1,#], Siyao Gu[3,#], Hui-hui Yang[1], Weidong Xie[3,], Cheng Gao[1,*], Dayong Gu[1,*]*

[1]Department of Laboratory Medicine, Shenzhen Institute of Translational Medicine, The First Affiliated Hospital of Shenzhen University, Shenzhen Second People's Hospital, Shenzhen, 518035, China.

[2]Shenzhen Institute of Synthetic Biology, Shenzhen Institute of Advanced Technology, Chinese Academy of Sciences, Shenzhen, 518055, China.

[3]Shenzhen Key Laboratory of Health Science and Technology, Institute of Biopharmaceutical and Health Engineering, Shenzhen International Graduate School, Tsinghua University, Shenzhen 518055, China.

[*]Corresponding email:

xiewd@sz.tsinghua.edu.cn, chenggao@email.szu.edu.cn, wanhood@email.szu.edu.cn

[#]These three authors contributed equally to this work.

Materials and methods

Experimental design

The objective of this study is to employ intracellular gelation technology to preserve the original morphology and structure of target cells while rendering them non-functional, thereby creating specific gel cell traps for virus adsorption. We utilized PEG-DA and Irgacure 2959 (I2959) to prepare hydrogels through photochemical cross-linking. Through a successful process involving freezing, infiltration, and cross-linking, we prepared GCs and assessed its structural morphology, proliferation, stability, *in vivo* safety, and its capacity to protect target cells against viral infection.

Materials, cell lines, and animals

PEG-DA (molecular weight 700 Da) and I2959 were procured from Aladdin (China). DiD, Annexin-V-PI, and Crystal Purple were obtained from Biyotime (China). Penicillin-streptomycin (5000 U/mL), MEM, DMEM, trypsin, and fetal bovine serum (FBS) were purchased from Gibco (USA). The CVB3 Nancy virus strain was generously provided by Professor Chen Ruizhen of Fudan University and stored at -80°C. CVB3 was amplified in Hela cells, which were cultured in MEM medium supplemented with 10% FBS. Once the cell density reached approximately 80%, the supernatant was discarded, and 5 mL of serum-free culture medium and 100 μL of CVB3 were added. The cells were then incubated at 37°C with 5% CO_2. When the cytopathic effect (CPE)

reached 70%, the petri dish was frozen at -80 °C for 5 min, thawed at 37 °C, and subjected to three to four cycles of freezing and thawing. The supernatant was then centrifuged at 1000 rpm for 5 min to obtain the CVB3. The virus solution was diluted tenfold with 2% MEM, resulting in a total of ten dilutions. The diluted virus was added to pre-prepared Hela cells in a 96-well plate, with eight replicates for each dilution. The cells were cultured in a cell incubator for 5-7 days, and the number of CPE-positive wells was recorded under a microscope for each dilution. The TCID50 (tissue culture infective dose 50%) was calculated using the following formula: logTCID50 = log10 (virus dilution yielding 50% tissue culture infection) + distance ratio × log10 (dilution factor). Hela and HL-1 cell lines were purchased from Meisen and authenticated through DNA fingerprinting, isozyme detection, and mycoplasma detection. The cells were cultured in a medium containing 10% fetal bovine serum and passaged every 1-2 days. Balb/c mice (5-6 weeks old, male) were purchased from Charles River. All animal experiments were approved by the Animal Ethics Committee of Shenzhen Second People's Hospital and conducted in accordance with the Animal Management Rules of the Ministry of Health of the People's Republic of China.

Intracellular gelation of GCs

HL-1 cells were seeded in 15 cm cell culture dishes. When the cell density reached 80%, the supernatant was discarded, and the cells were washed twice with PBS. Next, 10 mL of a 10% PEG-DA and 0.1% I2959 solution was added to the dish. The cells were then frozen at -80°C for 10 min, followed by thawing at 37°C. The excess PEG-DA and I2959 in the supernatant were discarded. Subsequently, the cells were exposed to 6W UV irradiation for 15 min to induce gelation and form GCs. The GCs were collected using the scraping method, washed twice with PBS, and filtered through a 70 μm filter to remove any aggregated GCs, ensuring cellular uniformity. The prepared GCs were stored in PBS at a concentration of 1×10^6 cells/mL and stored

at 4°C.

Preparation of NS

HL-1 cells were initially washed twice with ice-cold 1 × PBS, then resuspended in a hypo-osmotic PBS containing 20 mM TrisHCl (pH = 7.5), 225 mM D-mannitol, 75 mM sucrose, 0.2 mM Ethylene glycol-bis (β-aminoethyl ether) - N,N,N',N' - tetraacetic acid (EGTA), and protease and phosphatase inhibitors. The cells were placed on ice and lysed with a homogenizer for 30 minutes. Subsequently, the mixture was centrifuged at 20,000g for 25 minutes at 4℃, discarding the pellet and centrifuging the supernatant at 100,000g for 35 minutes at 4℃ to collect the cell membrane precipitate. For the synthesis of nanoparticle cores, 400 μL of poly (50:50 PLGA, 0.67 dl/g; Lactel Absorbable Polymers) in acetone (20 mg/mL) was added dropwise into 1 mL of water until all the acetone had evaporated. Then, the polymer was mixed with the HL-1 cell membrane at a weight ratio of 2:1, followed by 2 minutes of sonication in a water bath to yield the nanoparticles (NS).

Characterization of GCs

Cell morphology was observed using a light microscope, scanning electron microscope (SEM, SU8100, Japan) and transmission electron microscopy (TEM, Talos L120C, Germany) for live cells, NGDs, and GCs. The prepared cells were directly observed using an ordinary light microscope. For SEM imaging, the samples were washed with PBS and fixed with an electron microscope fixative at room temperature for 2 h, followed by transfer to 4°C for preservation. The fixed samples were then washed three times with 0.1M PBS (pH 7.4) and fixed with 1% osmium tetroxide in the dark at room temperature for 1-2 h. After three additional washes with 0.1M PBS (pH 7.4) for 15 min each, the cells were dehydrated in a series of ethanol solutions (30%, 50%,

70%, 80%, 90%, 95%, and 100%) for 15 min each. Subsequently, the cells were treated with isoamyl acetate for 15 min, dried, and made conductive. Finally, images were captured using the scanning electron microscope. For TEM imaging, 10 μL of the cell sample is pipetted onto a carbon-coated copper grid and left for 2 min, then the excess liquid is removed with filter paper. 10 μL of uranyl acetate is applied to the copper grid for 1 min, and the excess liquid is removed with filter paper, followed by drying at room temperature, images are collected for analysis.

The staining of the DiD membrane was observed using confocal microscope. Cells from the live group, NGD group, and GC group were washed twice with PBS in confocal dishes. Then, 1 mL of 400× DiD dye was added to each well. After incubating at 37°C for 20 s, the cells were washed three times with PBS and observed using a confocal microscope. The excitation wavelength used was 644 nm, and the emission wavelength was 665 nm.

The diameter of cells in each group was measured using a cell counter. A 10 μL aliquot of cells was taken and mixed with trypan blue at a 1:1 ratio. After allowing the cells to stabilize, the diameter was measured using a cell counter.

SDS-PAGE electrophoresis was performed to detect the protein components of cells in each group and determine if there was any loss of membrane proteins. The protein from each group of cells was extracted, and its concentration was determined using BCA. The protein samples from each group were heated to 95°C for 5 min. Then, 30 μg of the samples were loaded onto a 10% gel and electrophoresed at 120 V for 2 h. After electrophoresis, the gel was stained with Coomassie brilliant blue dye for 2 h and washed overnight before imaging.

Add 1mL of 4% paraformaldehyde to the confocal dish and incubate at room temperature for

20 min. Then add 0.1% Triton to permeabilize the membrane for 20 min, followed by washing 3 times with PBS. Add 3% BSA and incubate at room temperature for 30 min to block non-specific binding, then add the primary antibody against α-actin and incubate overnight at 4°C in a humidified chamber. Wash 3 times with PBS, each time for 10 min. Add the secondary antibody conjugated to GFP and incubate at room temperature for 1 hour, then wash on a shaker 3 times, each time for 10 min. Add DAPI at a 1:1000 dilution and incubate at room temperature for 5 min, then wash 3 times with PBS. Fluorescence signals are collected using a confocal microscope, with excitation wavelengths for DAPI at 330-380 nm and emission wavelength at 420 nm; for GFP, the excitation wavelength is 465-495 nm, and the emission wavelength is 515-555 nm.

Cell viability was assessed using the CCK8 assay. HL-1 cells and GCs cells (5000 cells) were seeded in 96-well plates, and the absorbance at OD405 was measured at 24 h, 48 h, and 72 h. Additionally, the effect of GCs on the growth of living cells was also evaluated using the CCK8 assay. HL-1 cells (5000 cells) were seeded in 96-well plates and co-cultured with different ratios of GCs (1:10, 1:1, 10:1). After 24 h, 48 h, and 72 h, the GCs cells in the supernatant were washed off, and then 100 μL of DMEM and 10 μL of CCK8 were added. The plates were incubated in the dark for 1 h at 37°C, and the absorbance at OD405 was measured.

Flow cytometry was employed to detect cell death. The cell concentration in both groups was adjusted to 1×10^5 cells in a volume of 100 μL and washed twice with PBS. Then, 5 μL of Annexin-V-GFP and PI-PE were added to the cells. After incubating at room temperature for 10 min, the cells were analyzed using flow cytometry. Double positive results indicated cell death.

In vitro evaluation of the ability of GCs to prevent CVB3 infection in cells

Hela and HL-1 cells were cultured in 6-well plates at a density of 1×10^6 cells per well. When the cell density reached 60%, the positive control group was treated with 100 TCID50 CVB3,

while the experimental group was treated with 100 TCID50 CVB3 along with either NGDs or GCs. The cells were incubated at 37°C for 2 h, followed by two washes with PBS and incubation with fresh culture medium for 24 h. Total RNA from the cells was extracted using the FastPure® Cell/Tissue Total RNA Isolation Kit V2. The CVB3 mRNA level in each group was then detected by RT-PCR using the Takara PrimeScriptTM RT reagent Kit with gDNA Eraser and TB Green® Premix Ex TaqTM II kits. The primer sequences for the RT-PCR are as follows (5'-3' sequences)：

CVB3 forward	GTGGTGGGCTATGGAGTATG
CVB3 reverse	ATTGCACAGAGTCAAGGGT
h-β-actin forward	CTCCATCCTGGCCTCGCTGT
h-β-actin reverse	CTCCATCCTGGCCTCGCTGT

GCs can inhibit CVB3 infection, primarily because they are essentially cardiomyocytes that have lost the ability to proliferate. Considering that GCs might suppress CVB3 infection by forming a physical barrier between the host cells and the GCs, one approach is to pre-incubate GCs with different concentrations of CVB3 and then infect Hela cells. Another approach is to pre-incubate the GCs with the virus for 30 min and then use the supernatant for infection. The virus plaque assay was performed to assess the infectivity of the virus on target cells. For this experiment, Hela and HL-1 cells were seeded in 6-well plates at a density of 1×10^6 cells per well. When the cell density reached 90%, the viral plaque assay was conducted. The negative control group was treated with DMEM medium only, the positive control group was added with 100 TCID50 CVB3, and the experimental group was added with 100 TCID50 CVB3 along with either NGDs or GCs. The cells were incubated in a cell incubator for 1 h with intermittent shaking every 15 min. Next, 3% agarose solution was prepared and heated to 45°C. 0.3% agarose solution was prepared in 10%

FBS DMEM and added to each well after washing the cells with PBS twice. The cells were then incubated in a 37°C, 5% CO_2 incubator for 60-84 h until clear cytopathic effect (CPE) was observed. Subsequently, 1mL of 4% paraformaldehyde was added to each well and left at room temperature for 6-12 h to allow for fixation. The agarose was then rinsed off with running water, and each well was stained with 1mL of crystal violet dye at room temperature for 20 min. After washing with PBS for 2-3 times, pictures were taken, and the number of plaques was calculated.

GCs biodistribution study

In vitro experiments were conducted using pre-prepared NGDs and GCs. DiD fluorescent dye was used for cell membrane staining. The exciting light was 644 nm, and the emitted light was 665 nm. For *in vivo* distribution studies, Balb/c mice were selected to evaluate the metabolism of GCs. On day 0, intravenous injections of NGDs and GCs were administered at a concentration of 5×10^5 cells in a volume of 150 μL. Considering the potential risk of pulmonary embolism and associated mortality when injecting NGDs at a concentration of 1×10^6 cells in a volume of 150 μL, the dosage was reduced by half to 5×10^5 cells in a volume of 150 μL. Subsequently, live imaging of the mice was conducted at 24 h, 48 h, and 72 h post-injection to monitor the fluorescence signal. Furthermore, the heart, liver, spleen, lungs, and kidneys were collected to detect the fluorescence signal, indicating the distribution of GCs in these organs.

HL-1 cells are stained with DiD, and then NS and GCs are prepared. For the *in vivo* distribution experiment, Balb/c mice are selected to evaluate the metabolism of GCs. On Day 0, 150μL of NS (prepared from 1×10^7 cardiomyocytes) and GCs (1×10^6) are injected intravenously. At 6 h, 12 h, 24 h, 48 h, 72 h, 96 h, and 120 h after injection, live imaging is performed on the mice to monitor the fluorescence signal. In addition, the heart, liver, spleen, lungs, and kidneys are collected to detect the fluorescence signal, in order to understand the distribution and metabolism of GCs in

these organs.

In vivo safety studies and the evaluation of the ability of GCs to prevent CVB3 infection in VMC mice

In vivo safety studies were conducted using Balb/c mice to assess the biocompatibility of GCs. GCs were administered i.v. at a concentration of 1×10^6 in a volume of 150 μL every other day for a total of four injections. Blood samples were collected through cardiac puncture, with 100 μL of peripheral blood collected using an EDTA anticoagulant tube for a complete blood count. Blood biochemical indexes were measured using a separation gel coagulant tube, and 500 μL of peripheral blood was centrifuged at 3000 rpm to obtain serum.

The heart, liver, spleen, lungs, and kidney tissues from all mice were fixed in 4% paraformaldehyde for 24 h. Afterward, the tissues were dehydrated, embedded in paraffin, and sectioned into 5 μm slices. Hematoxylin and eosin (H&E) staining was performed, and the images were captured using a slide scanning image system (SQS-40P). The images were then analyzed using caseviewer software. The experiment to inhibit CVB3-induced viral myocarditis (VMC) in mice with GCs was divided into two parts. The first part is on day 0, 30 mice were randomly divided into five groups: negative control (NC), CVB3, PEG-DA+I2959 (P+I), GCs, and Ribavirin groups. Except for the NC group, each mouse was intraperitoneally injected with 1×10^5 TCID50 of CVB3, and their body weight was recorded. Starting from day 2, tail vein injections were administered every other day. It should be noted that the amount of P+I used was equivalent to that permeated into the GCs, and the mixture also underwent 15 min of ultraviolet irradiation and was added with the same amount of PBS as the diluted GCs. The cell concentration in the GCs group was 1×10^6 cells in a volume of 150 μL, and the dose of Ribavirin was 100 mg/kg. The subsequent experimental scheme followed the same protocol as the *in vivo* safety experiment. The

other part is on day 0, 45 mice were randomly divided into five groups: NC, CVB3, NS, GCs, and Ribavirin groups. Except for the NC group, each mouse was intraperitoneally injected with 1×10^5 TCID50 of CVB3, and their body weight was recorded. Starting from day 2, tail vein injections were administered every other day for a total of 7 injections. On day 7, we evaluated CVB3 viral load, IFN-β, IFN-γ, Fas expression levels related to myocardial cell damage, and serum indicators closely related to viral infection (cTnI, CK, CK-MB, LDH, and LDH-L). On day 3, day 7 and day 14，we collected heart, liver, spleen, lungs, and kidneys of mice for pathological analysis。

Statistical analysis

Student's t test was used for comparison between two columns of date. One-way analysis of variance(ANOVA) was used where three or more columns of data were compared. Two-way ANOVA were utilized where two or more columns of data were compared. Values of *P $\leqslant$ 0.05, **P $\leqslant$ 0.01 and ***P $\leqslant$ 0.001 were considered statistical significance. All experiments were repeated at least three times, and all data was shown as the mean ± standard deviation (SD).

Supplementary Figures

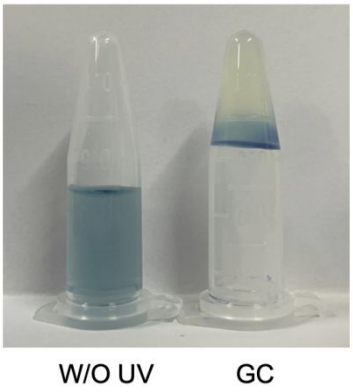

Figure S1. Characterization of hydrogel. Photograph of hydrogel prepared from 10 wt% of PEG-DA and 1 wt% of I2959 with or without UV irradiation (6W) for 15 min.

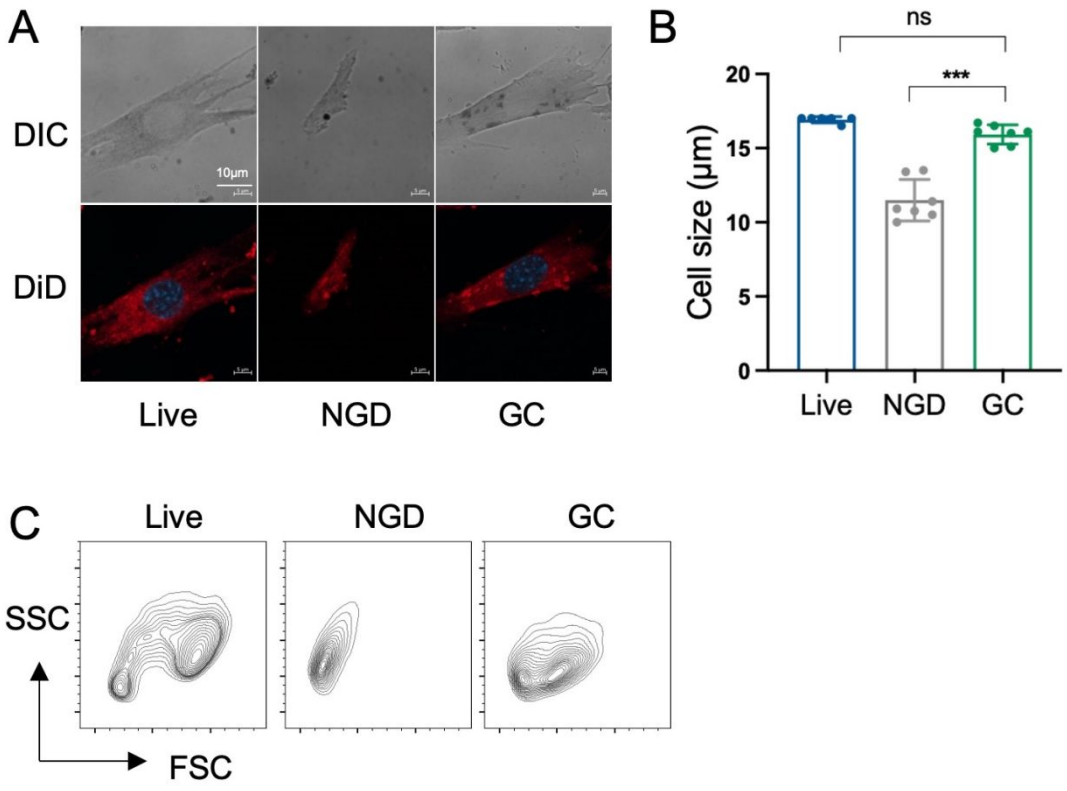

Figure S2. Characterization of GCs. (A) Representative fluorescence imaging on GCs by DiD membrane staining. Cell morphology was observed using confocal microscope. (B) Measurement of cell diameter by hematocytometer. (C) Representative flow cytometry scatter plots of Live cells, NGDs and GCs.

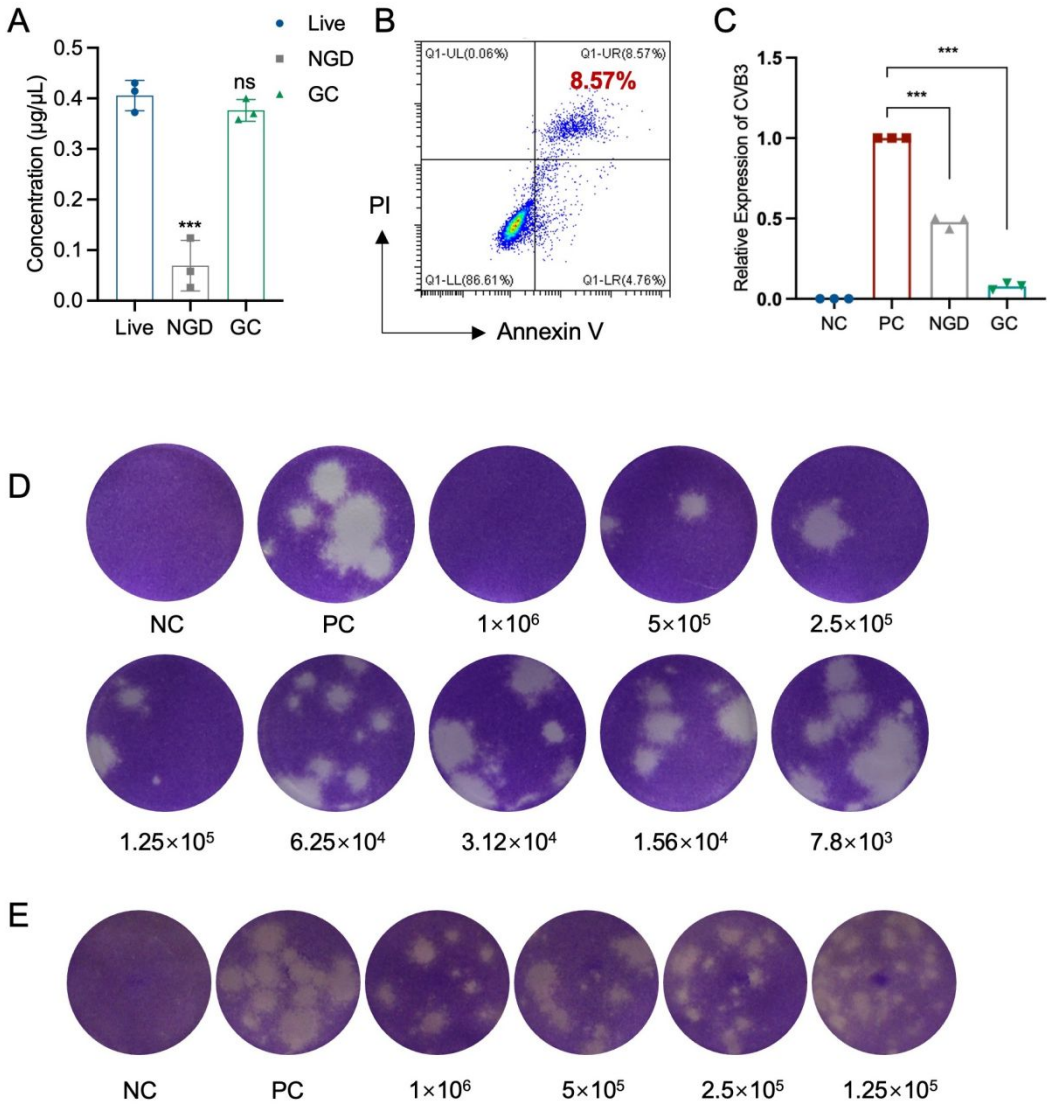

Figure S3. GCs inhibited CVB3 infection in host cells. (A) Protein concentration (BCA) of Live, NGD and GC cells. (B) Detection of cell death in live cell group using Annexin V/PI double staining and flow cytometry. (C) RT-PCR detection of CVB3 RNA levels in HL-1 cells with or without the addition of NGDs and GCs. NC: Negative control; PC: Positive control with CVB3 virus. (D) Plaque morphology of CVB3 in Hela cells with or without the addition of GCs diluted at a 1/2 concentration. (E) GCs were pre-incubated with virus for 30 min and then used the supernatant for infection. Plaque morphology of CVB3 in Hela cells. NS = non-significant, **P $\leqslant$ 0.01, and ***P $\leqslant$ 0.001.

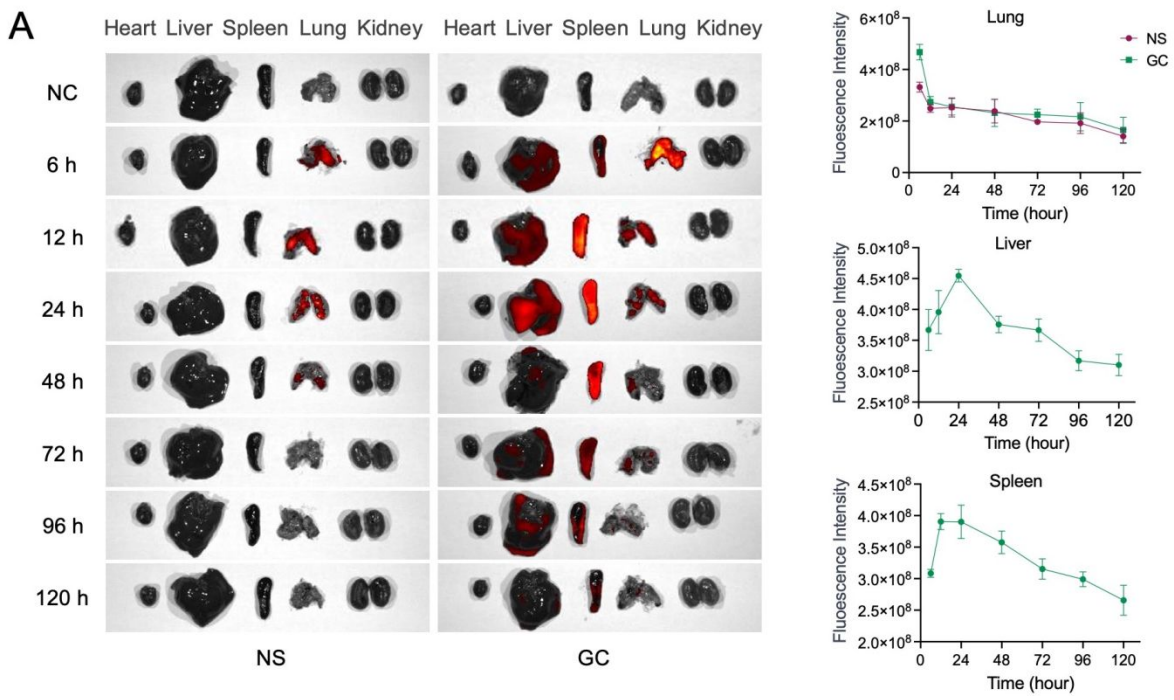

Figure S4. *In vivo* distribution experiment. (A) Healthy mice were i.v. injected with NS (prepared from 1×10^6 cardiomyocyte) and GCs (1×10^6) per mouse, and the fluorescence signals of heart, liver, spleen, lung, and kidney were detected using *in vivo* imaging system at 6 h, 12 h, 24 h, 48 h, 72 h, 96 h, and 120 h (n = 7).

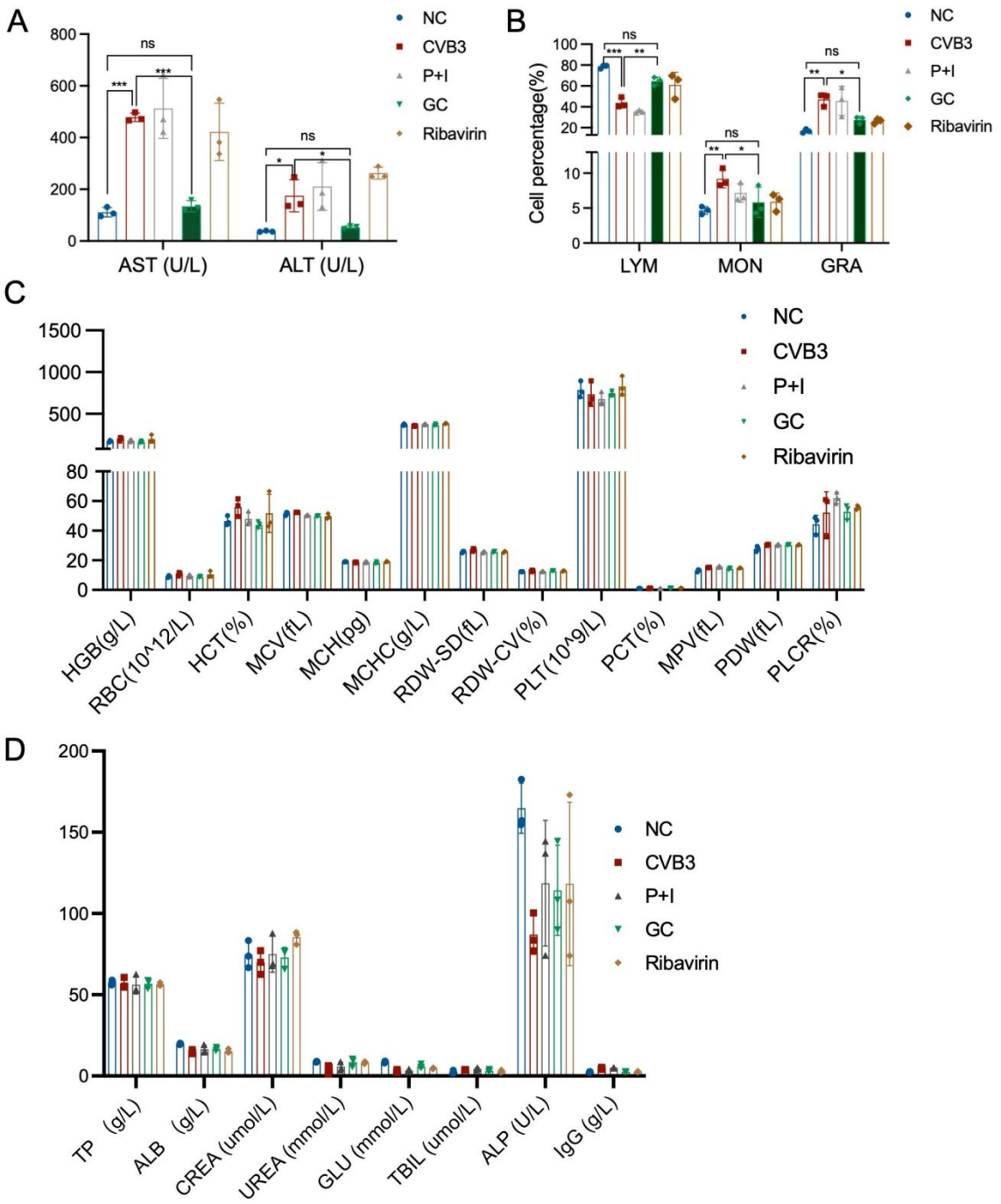

Figure S5. *In vivo* therapy of GCs against CVB3 infection. (A) Serum levels of AST and ALT. (B) Blood cell proportions of lymphocyte (LYM), monocyte (MON), and granulocyte (GRA). (C) Complete blood count performed at day 7. (D) Comprehensive serum chemistry panel performed at day 7. NS = non-significant, **P $\leqslant$ 0.01, and ***P $\leqslant$ 0.001.

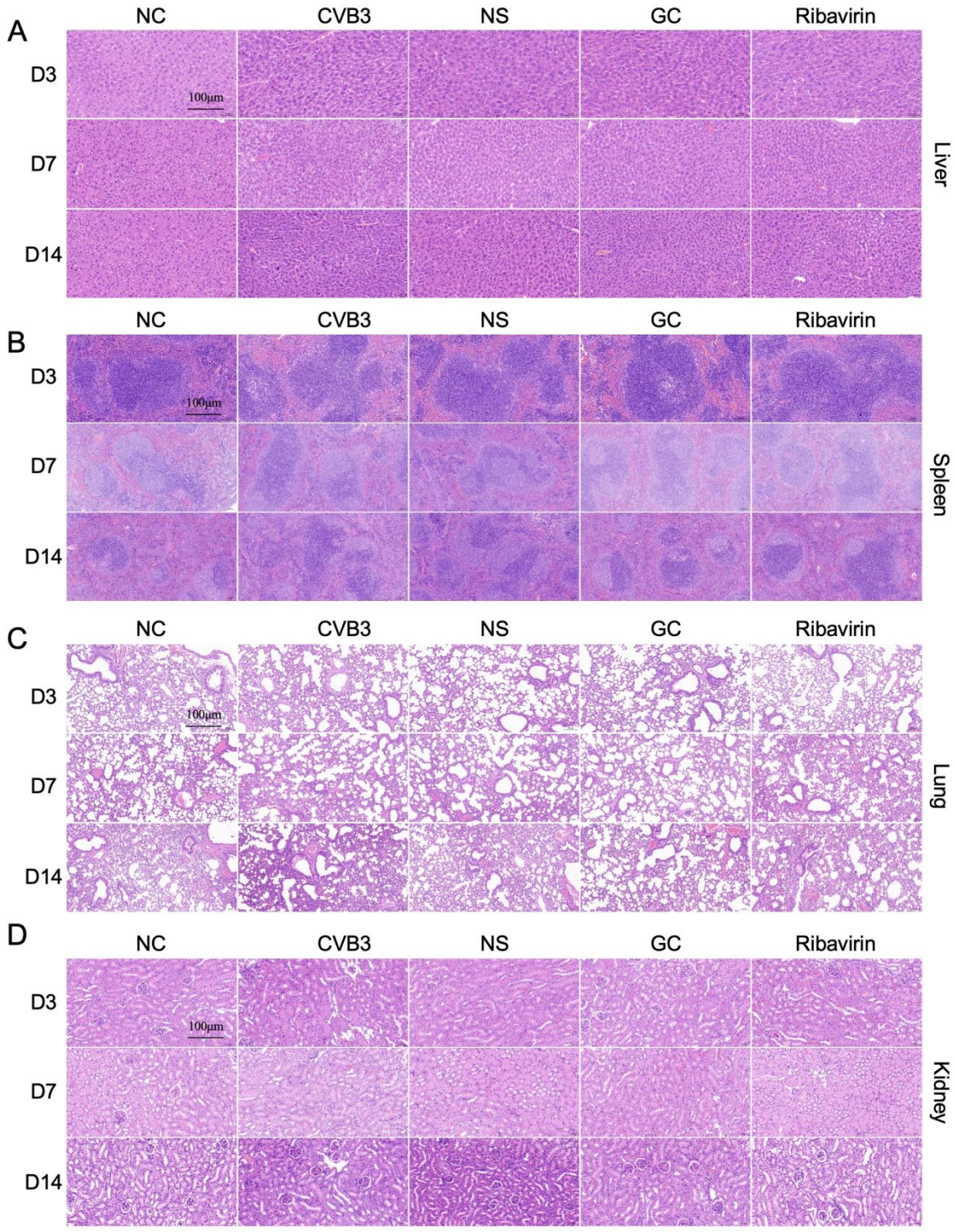

Figure S6. Histopathological analysis of liver (A), spleen (B), lung (C), and kidney (D) using H&E-stained tissue sections on day 3, day 7, and day 14.